

1 **PRAG3674_22-030R2**

2 **Improved estimation of herbaceous crop aboveground biomass using UAV-derived crop**
3 **height combined with vegetation indices**

4 Martina Corti¹, Daniele Cavalli^{1,2}, Giovanni Cabassi², Luca Bechini¹, Nicolò Pricca², Dario
5 Paolo^{2,3}, Laura Marinoni⁴, Antonio Vigoni⁵, Luigi Degano², Pietro Marino Gallina¹

6 ¹ Department of Agricultural and Environmental Sciences-Production, Landscape, Agroenergy,
7 Università degli Studi di Milano, via Celoria 2, 20133 Milano, Italy;

8 ² CREA - Council for Agricultural Research and Economics, Research Centre for Animal
9 Production and Aquaculture, via Antonio Lombardo 11, 26900 Lodi, Italy;

10 ³ CNR - Consiglio Nazionale delle Ricerche, Institute of Agricultural Biology and Biotechnology
11 (IBBA), Via Edoardo Bassini 15, 20133 Milano, Italy;

12 ⁴ CREA - Council for Agricultural Research and Economics, Research Centre for Engineering and
13 Agro-Food Processing, via Giacomo Venezian 26, 20133 Milano, Italy;

14 ⁵ Sport Turf Consulting-Servizi per l'agricoltura con aeromobili a pilotaggio remoto, Via Cesare
15 Battisti, 19, 20027 Rescaldina, MI, Italy;

16 Corresponding author: Martina Corti, martina.corti@unimi.it

17 **ABSTRACT**

18 Vegetation indices are used in precision agriculture to estimate crop aboveground biomass (AGB),
19 and, in turn, to quantify crop needs. However, crop species and development stage affect vegetation
20 indices limiting the setup of generalized models for AGB estimation. Some approaches to overcome
21 this issue have combined vegetation indices and structural crop properties such as crop height.
22 However, only a few studies have considered different herbaceous crops like forages and cover
23 crops. A two-year field experiment was carried out on five winter cover crops with different habits
24 at a high cover fraction (on average 93%) to study if combining vegetation indices, crop height and
25 the fraction of soil covered by the crop could improve AGB estimation. Seven vegetation indices,
26 crop height and cover fraction were derived from UAV-multispectral images. Species-specific and
27 global (including all species) regression models were built and tested through cross-validation
28 (CV). Green-based indices were the best estimators of AGB ($R_{CV}^2= 0.56-0.93$, normalized root
29 mean square error in CV $nRMSECV= 26-38\%$) of the five species, separately. A global linear
30 model using crop height alone, provided good results ($R_{CV}^2= 0.57$, $nRMSECV= 42\%$). Also,
31 stepwise multiple regression was used to get a global model with crop height and five vegetation
32 indices ($R_{CV}^2= 0.75$, $nRMSECV= 31\%$). Finally, a model was proposed where AGB was estimated
33 by a vegetation index until plants covered 97% of soil or its height was shorter than 125 mm, and
34 by crop height for vegetation taller than 125 mm. The promising results ($R_{CV}^2= 0.65$, $nRMSECV=$
35 37%) suggested the possibility of increasing AGB estimation by considering both UAV-derived
36 vegetation indices and structural crop properties.

37 **KEYWORDS**

38 Crop surface models, multispectral camera, reflectance, cover crops

39 **ACKNOWLEDGMENTS**

40 The experiment was part of the CoCrop project (CUP E86G16002800007), funded by the European
41 Agricultural Fund for Rural Development (EAFRD) under Measure 16, Operation 16.2.01, of the
42 Rural Development Program 2014-2020 of the Lombardy Region (Italy). The authors thank the
43 students and collaborators who helped in field work and sampling campaigns: Fabio Introzzi,
44 Roberto Fuccella, Riccardo Asti, Matteo Bosso, Federico Concas, Michele Croci, Stefano
45 Virgadola, Davide Mapelli, Paolo Pozzi, Pietro Zarpellon, Riccardo Beretta. Thanks to Virginia
46 Fassa for her help in map visualization.

47 INTRODUCTION

48 Since its first applications, remote sensing of vegetation has been used to characterize the type,
49 amount and status of plants (Jackson and Huete, 1991). Such pieces of information have their main
50 use in crop production especially in precision agriculture, where quick and spatialized detection of
51 crop status is needed to guide site-specific crop management. Agricultural applications mainly
52 involve the use of optical sensors able to record the relative amount of electromagnetic energy that
53 is reflected or transmitted by the vegetation. This energy mainly gives information about leaf
54 chlorophyll content (in the visible, red-edge regions) and leaf structural properties (in the near-
55 infrared, NIR), that are linked to plant nutrient and water status, respectively (Corti et al., 2017).
56 Spatialized reflectance data must be recorded quickly and on-demand to be satisfactorily used in
57 operational conditions. Therefore, contactless multispectral sensors carried by tractors (such as
58 CropCircle, Yara-N-sensor, GreenSeeker) and imaging sensors (multispectral cameras) airborne
59 (often mounted on unmanned aerial vehicles, UAV) or satellite-mounted (Muñoz-Huerta et al.,
60 2013) are the most used.

61 Measured reflectance values in the visible and NIR bands are linearly or non-linearly combined to
62 calculate vegetation indices (Huete et al., 1997; Pinter et al., 2003). Since their first applications,
63 vegetation indices have been shown to be affected by different factors such as the sensor type,
64 background, atmospheric conditions, sensor view and solar angles (Jackson and Huete, 1991) but
65 also by leaf color and canopy architecture (Pinter et al., 2003) that depend on crop species, variety
66 and development stage and biotic and abiotic factors (Thenkabail et al., 2000). Most of the issues
67 related to sensors and to external conditions during the acquisition of spectral data found different
68 solutions *e.g.*, setup of specific ambient conditions during spectra acquisition (Pauly, 2016;
69 Rasmussen et al., 2016), the use of reference panel for radiometric calibration (Pauly, 2016),
70 background noise removal (Noh et al., 2005), specific vegetation indices that mitigate background
71 or atmospheric interferences (Mutanga and Skidmore, 2004). However, regardless of the type of
72 vegetation index used and the crop species under study, both the saturation phenomenon (*i.e.*,

73 vegetation indices reach their maximum values when the crop is still growing, and therefore, at high
74 vegetation cover fraction, vegetation indices underestimate crop biomass) and the effects of variety
75 and development stage do not allow the development of empirical regression models estimating
76 crop biophysical properties based on vegetation indices that are of general validity (Corti et al.,
77 2018). They also could compromise other important applications of vegetation indices such as
78 algorithms to support decision-making in site-specific crop management (Corti et al., 2020).

79 Some attempts to overcome saturation and specificity of vegetation indices were made by proposing
80 new vegetation indices (Haboudane et al., 2002), by combining vegetation indices (Gu et al., 2013),
81 or by proposing multivariate approaches that consider different wavelengths (Bendig et al., 2015).

82 At the same time, advances in remote sensing led to the estimation of other variables more linked to
83 crop structural properties such as crop height (Jimenez-Berni et al., 2018) and canopy volume
84 (Calou et al., 2019), thanks to the development and the diffusion of new sensors such as LiDAR,
85 multispectral imaging sensors for photogrammetry mounted on UAV, 3d reconstruction and
86 ultrasonic sonars. Specifically, crop height is well known to be related to crop biomass within crop
87 species (Madec et al., 2017) and final yield (Bendig et al., 2015). Moreover, it accounts for crop
88 nitrogen and water stress (Azimi et al., 2021; Madec et al., 2017). For these reasons, the literature
89 has focused on proving the ability of new sensors and on data analysis techniques to provide good
90 estimates of crop height; various sensors and techniques have been proposed and compared on
91 different crops (Madec et al., 2017; Roth and Streit, 2018). Despite the great importance of crop
92 height in describing crop status, only a few studies have verified the opportunity of integrating it
93 with vegetation indices in order to improve the prediction of crop biomass (Sharma et al., 2016)
94 using, specifically, plant height obtained from digital cameras mounted on UAVs. These studies
95 adopted different approaches like the correction of vegetation indices by multiplication with crop
96 height (Freeman et al., 2007), and the use of multiple regression models (Bendig et al., 2015).

97 However, published works have focused on grain crops like cereals (Freeman et al., 2007; Bendig et

98 al., 2014; Tilly et al., 2015), while herbaceous crops, cultivated for their leaves and stems (forage
99 and cover crops), have rarely been the subject of these studies.

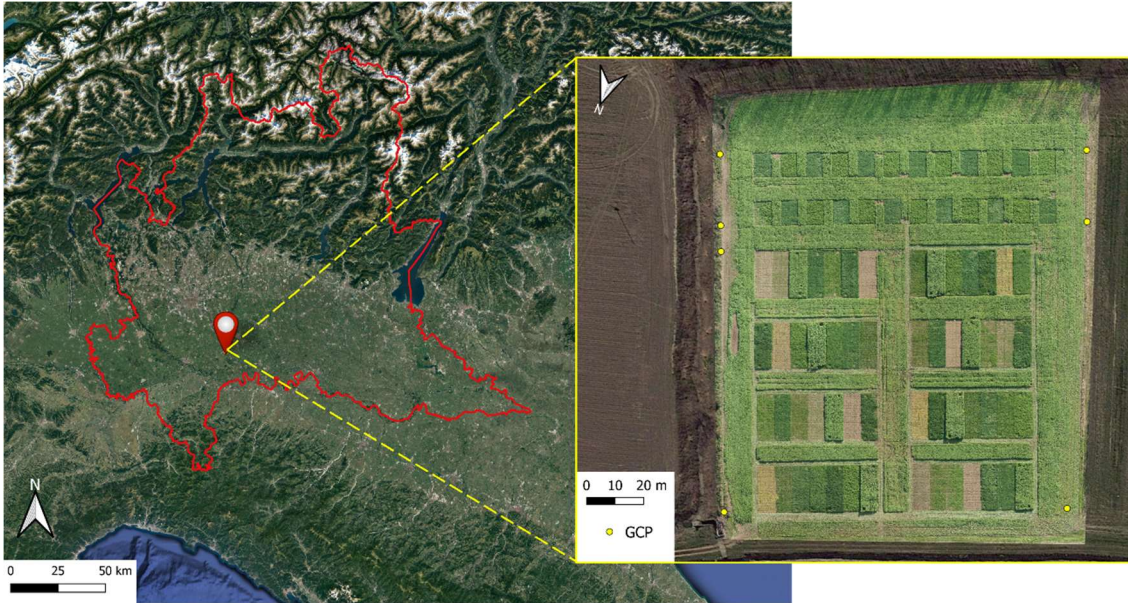
100 Therefore, the objective of this research was to verify if combining UAV-derived crop height with
101 various commonly used vegetation indices could improve the estimation of aboveground biomass of
102 herbaceous crop species having different plant habits, using data from a two-year experiment on
103 five forage and cover crop species.

104 **MATERIALS AND METHODS**

105 **Experimental field**

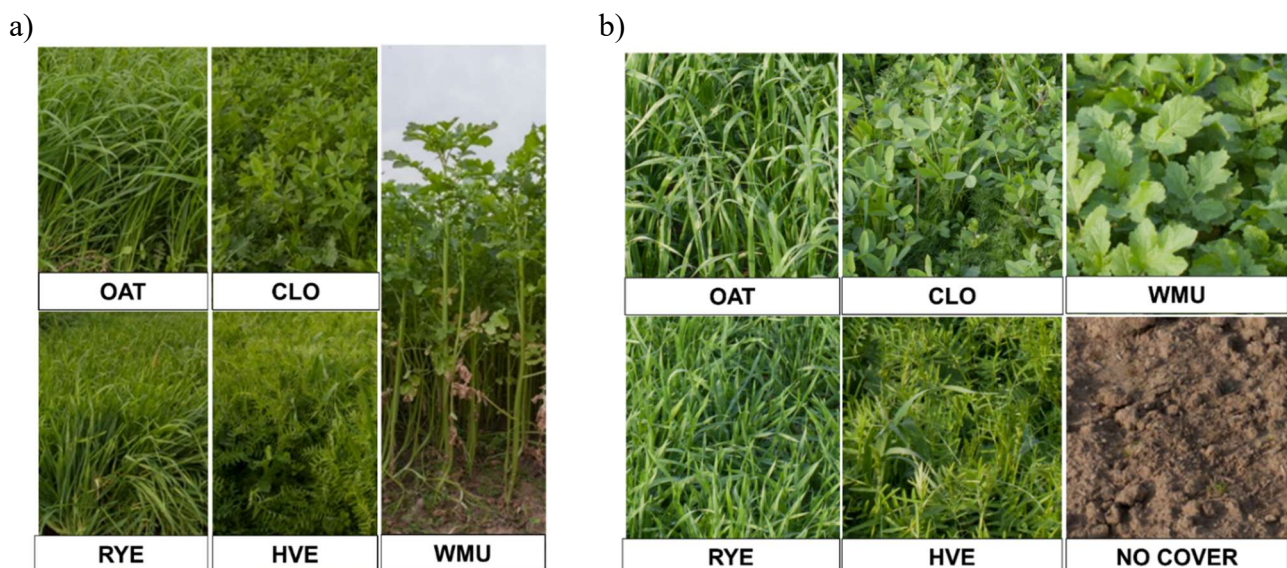
106 The study was carried out in an experimental field of 1.6 ha located in Sant'Angelo Lodigiano
107 (Lodi), Italy, at Cascina Santa Martina of Morando Bolognini Foundation (45° 13' 57.6" N, 9° 25'
108 36.7" E, altitude 73 m asl), during 2017 and 2018 growing season. The field hosted an experiment
109 on winter cover crops (Fig. 1) aimed at studying the effects of crop species, date of sowing and
110 maize post-harvest soil mineral nitrogen on aboveground biomass production and nitrogen removal
111 of cover crops and cover crops competition with weeds. The experimental factors were crop
112 species, date of sowing and post-harvest soil mineral nitrogen. Five cover crops species were
113 compared: two grasses, *Avena strigosa* Schreb. Saia variety (black oat, OAT) and *Secale cereale* L.
114 Stanko variety (rye, RYE); two legumes, *Vicia villosa* Roth Villana variety (hairy vetch, HVE) and
115 *Trifolium alexandrinum* L. Mario variety (Egyptian clover, CLO); and a cruciferous, *Sinapis alba*
116 L. Architect variety (white mustard, WMU). In addition, weeded and non-weeded control
117 treatments were included. Two sowing dates (6th and 22nd September of both 2017 and 2018) and
118 two application rates of nitrogen were tested: 0 kg N ha⁻¹; and 50 kg N ha⁻¹ year⁻¹ as calcium nitrate
119 applied before sowing the cover crops. The experimental factors were combined according to a
120 complete factorial design with four replicates (blocks) arranged in a hierarchical split-split plot
121 design with sub-sub plots of 48 m² each (6x8 m). The field experiment provided a large dataset (N
122 = 240, as a result of the factorial combination of 5 species × 2 sowing dates × 2 soil N × 4 replicates

123 × 3 campaigns of crop samplings), characterized by great variability in aboveground biomass
124 generated by the combination of the experimental factors and great variability of the five crop
125 habits.



126
127 **Fig. 1** Experimental site in Lombardy and focus on the ortho-image of the experimental field
128 captured by a Sony a6000 camera in October 2017. Yellow dots represent the positions of the seven
129 ground control points (GCP).

130
131 Fig. 2 shows images with front and top views of the plots to give an example of the different plant
132 architectures and soil coverage of the tested cover crops.



133 **Fig. 2** Front (a) and top (b) views of the cover crops: black oat, OAT; rye, RYE; hairy vetch, HVE;
134 Egyptian clover, CLO; and white mustard, WMU.

135

136 The soil of the field was flat and with homogeneous properties and characterized by 45% sand, 41%
137 silt and 14% clay, by the absence of skeleton, by sub-acid reaction ($\text{pH H}_2\text{O} = 6.0$) and 1.5% organic
138 matter. The climate of Sant'Angelo Lodigiano is characterized by annual average precipitation of
139 830 mm and an average temperature of 13.2°C . During the year 2017, on 10th October, irrigation
140 was done in order to prevent water stress due to scarce precipitation in that period.

141 Aerial surveys

142 Aerial surveys of the field were made at three different dates in order to be able to monitor the
143 highest levels of cover crop growth: 30th October 2017, 20th November 2017 and 18th November
144 2018. A handmade coaxial octocopter, with a maximum takeoff mass of 12 kg and equipped with a
145 GNSS (Global Navigation Satellite System) NEOM8N (ublox, Thalwil, Switzerland) and a gimbal
146 platform-mounted multispectral MicaSense Red-edge camera (sensor resolution: 1.2 MP per band;
147 MicaSense, Inc., Seattle, WA, USA) which is a professional digital camera for agriculture
148 applications. It acquires reflectance in a blue band ($475 \pm 20 \text{ nm}$); a green band ($560 \pm 20 \text{ nm}$); a red
149 band ($668 \pm 10 \text{ nm}$); a red-edge band ($717 \pm 10 \text{ nm}$); a near-infrared band ($840 \pm 40 \text{ nm}$). The images
150 of a white reference panel (Spectralon®) were acquired before and after each flight in order to
151 perform radiometric calibration of the images. Nadir images of the fields were collected at an
152 altitude of 60 m, at solar noon, with a clear sky. The solar elevation angles were low ranging from
153 24° for the surveys made in November to 29° for the October 2017 survey, while solar Azimuth
154 varied between 192° and 194° , respectively. The flight plan guaranteed 85% of forward and
155 sideward overlap, needed for image processing.

156 Photogrammetry and image processing

157 Pix4Dmapper software (version 4.3.33; Pix4D SA, Lausanne, Switzerland) was used to build the
158 ortho-mosaics and the crop surface models (CSMs) of the experimental field. The ortho-mosaics of
159 the five bands recorded were built to calculate the maps of vegetation indices; the CSMs were built
160 in order to estimate crop height. Specifically, CSM is a raster file that represents the Earth's surface
161 including objects on it (*i.e.*, crop plants) and it was built with the following settings of
162 Pix4Dmapper software: noise filtering and surface smoothing were applied on the points cloud, and
163 the triangulation method was used to produce the raster files. The outputs of the processed images
164 consisted of five different reflectance TIFF images (16bit grayscale per band) and one crop surface
165 model (TIFF file) for each field survey. Ortho-imageOrtho-images and CSMs had a spatial
166 resolution of 4 cm.

167 The GNSS position (precision 0.012 m) of seven artificial targets (ground control points taken with
168 the Topcon GRS-1 GNSS RTK Receiver; TopCon Corporation, Tokyo, Japan) was used for
169 geometric correction (Fig. 1). Finally, the software QGIS (version 3.10; QGIS.org 2020) was used
170 to calculate UAV-based variables *i.e.*, estimated crop height, vegetation indices and vegetation
171 cover fraction. These variables were extracted, for each sampling date, by sampling in each ortho-
172 image and CSM, from a 1 m² area (as polygonal shapefile) positioned in the center of each plot.

173 *Structural crop properties: estimation of UAV-derived crop height and vegetation cover* 174 *fraction*

175 Crop height was estimated (Hest) from CSMs. Since the CSM measures the altitude of Earth plus
176 the crop on its surface, Hest was calculated as the difference between the altitude of the crop
177 (calculated as the 95° percentile of the altitude of each plot and bare soil). The altitude of the bare
178 soil was retrieved by sampling the CSM of chemically weeded plots, used as reference of bare soil.
179 Within each sampling campaign, a single reference soil altitude was used for the whole field and
180 was set to the mean of all bare soil plots (n= 16, corresponding to treatments without cover crops,
181 uniformly spread on the experimental field; Fig. 2). The altitude of bare soil was checked in every

182 CSM and it showed random differences (< 15 cm) indicating a flat field, characterized by the
 183 absence of a soil slope across plots. Moreover, soil compaction in non-weeded control plots was the
 184 same as that in crop plots because all agronomic operations potentially causing soil compaction
 185 (including seeding) were applied on cropped and control plots.

186 The vegetation cover fraction (FC) of the crops was calculated in every plot of each ortho-image. A
 187 threshold was established on the red-edge band by using the function *graythresh* that implemented
 188 the Otsu algorithm (Otsu, 1975) in MATLAB software (version 2014b, the Mathworks, Inc., MA,
 189 USA). The procedure provided a binary image separating plants from their background, by
 190 producing a black and white image where white pixels belong to vegetation and black pixels are the
 191 pixels of soil. Then, the FC was calculated for each plot as the ratio between the number of white
 192 pixels and the total number of pixels in the plot.

193 *UAV-derived vegetation indices*

194 Seven vegetation indices were calculated for each plot: two red-based indices, the normalized
 195 difference vegetation index (NDVI) and the optimized soil adjusted vegetation index (OSAVI); two
 196 green-based indices, the green normalized difference vegetation index (GNDVI) and the
 197 chlorophyll green index (CIg); two red-edge-based indices, the normalized difference red-edge
 198 index (NDREI) and the chlorophyll red-edge index (CIre); and one multiple-band vegetation index,
 199 the triangular vegetation index (TVI). These indices were chosen because they had been already
 200 tested in the literature for AGB estimation under high soil coverage on the species tested in this
 201 study or similar (Table 1).

202

203 **Table 1** Vegetation indices tested in this study. B, G, R, RE and NIR are the blue, green, red, red-
 204 edge and near-infrared bands recorded by the multispectral camera (MicaSense Red-edge).

<i>Vegetation index</i>	<i>Equation</i>
<i>NDVI</i>	$(\text{NIR} - \text{R})/(\text{NIR} + \text{R})$
<i>OSAVI</i>	$(1 + 0.16)(\text{NIR} - \text{R})/(\text{NIR} + \text{R} + 0.16)$

<i>GNDVI</i>	$(\text{NIR} - \text{G})/(\text{NIR} + \text{G})$
<i>CIg</i>	$(\text{NIR}/\text{G}) - 1$
<i>NDREI</i>	$(\text{RE} - \text{R})/(\text{RE} + \text{R})$
<i>CIre</i>	$(\text{NIR}/\text{RE}) - 1$
<i>TVI</i>	$0.5[(120(\text{NIR} - \text{G}) - 200(\text{R} - \text{G}))]$

205 Ground measurements

206 At the same dates as UAV field surveys, reference ground measurements of AGB and crop height
207 were taken. Plants of cover crops and weeds (if any) were harvested from 1 m² representative of
208 each plot. Cover crops and weeds were separated and weighed to collect their fresh weight. Then, a
209 sub-sample was oven-dried (105°C) until constant weight in order to obtain AGB values on a dry
210 weight (DW) basis of both cover crops and weeds. On the same day, the average height of plants on
211 1 m² was recorded using a graduated stick (precision 0.01 m) and a spirit level. Three measurements
212 per plot were taken close to the AGB sampling area, and they were averaged.

213 Data analysis

214 Data analysis was carried out using the R software (version 3.6.2; R Core Team, 2019). Descriptive
215 statistics of measured and UAV-based crop variables were calculated using *describe* and
216 *describeBY* functions of the “psych” R package (version 2.0.9; Revelle, 2020). Scatterplots were
217 made using the “ggplot2” R Package (version 3.3.5, Wickham, 2016).

218 Firstly, a simple regression model was built between ground-measured and UAV-derived crop
219 height in order to test the quality of the UAV estimation and to calculate the limit of quantification
220 (LOQ). The LOQ identifies the smallest ground-measured crop height that can be quantitatively
221 detected by the UAV. It is defined in Eq. 1 (Shrivastava and Gupta, 2001).

$$222 \text{LOQ} = 10 \frac{S_y}{m}$$

1

223 where S_y is the standard deviation of y-intercept and m is the slope of the linear regression model
224 between UAV-based crop height and ground-measured crop height. The bias of UAV-derived crop

225 height was also calculated as the difference between the mean of estimates and the true value of the
226 variable being estimated.

227 Then, simple regression models were fitted using *lm* function of the “R stats” package (version
228 3.6.2; R Core Team, 2019) to predict AGB from different predictors Hest, vegetation indices and
229 FC: linear fit, exponential fit and polynomial fits were tested. In addition, a multiple regression
230 model was built to combine the seven vegetation indices, Hest and FC in one global calibration
231 model, fitted for all species together. For this purpose, backward stepwise linear regression was
232 carried out using the “leaps” R package (version 3.1; Lumley, 2020).

233 Another regression method was adopted. It consisted of combining two regression models with the
234 following rules:

$$235 \text{ AGB} = f(\text{VI}) \quad \text{if } \text{FC} < \text{FC}_{\text{sat}} \text{ or } \text{Hest} \leq \text{LOQ} \quad 2$$

$$236 \text{ AGB} = f(\text{Hest}) \quad \text{if } \text{FC} \geq \text{FC}_{\text{sat}} \text{ and } \text{Hest} \geq \text{LOQ} \quad 3$$

237 Where $f(\dots)$ indicates the global calibration model with the best fit for the given predictor. The
238 FC_{sat} is the saturation of the vegetation cover fraction and it was defined by fitting a segmented
239 linear regression model between FC and AGB and finding the break-point (plateau). The
240 “segmented” R package (version 1.3-4; Muggeo, 2008) was used. At first, the whole dataset (all
241 species together) was divided into two parts accordingly to the values of the FC_{sat} and LOQ of Hest
242 (Eq. 1). Then, global calibration curves for each vegetation index (VI) were fitted separately and the
243 best regression model (either linear, exponential, or polynomial) was selected to estimate AGB
244 from VI until FC_{sat} occurs (Eq. 2), or if Hest is lower than the LOQ. Above saturation (Eq. 3),
245 AGB was estimated from a global calibration curve with Hest, only if it is greater than the LOQ.

246 *Statistics of the performances of regression models*

247 The simple and multiple regression models were tested by the contiguous block cross-validation
248 using the “caret” R package (version 6.0-90; Kuhn, 2021). The setting of cross-validation was
249 planned considering that the original experiment was arranged in four blocks of replicates.
250 Therefore, four folds were produced so that at every cancellation step, one block was used as the

251 test set. Since the dataset was composed of three dates of sampling in a two-year experiment, all the
 252 observations of all the years belonging to the same block were left out per cancellation group. The
 253 resulting sample size in cross-validation were: 36 samples in the training set and 12 samples in the
 254 test set for the species-specific regression models, 180 samples in the training set and 60 samples in
 255 the test set for the calibration of global models.

256 The determination coefficients in cross-validation (R_{CV}^2), the root mean square error in cross-
 257 validation (RMSECV), the normalized root mean square error in cross-validation (nRMSECV,
 258 represented by the RMSECV divided by the mean of the observed variable) and the mean absolute
 259 error in cross-validation (MAECV) of the fitted regression models were calculated.

260 RESULTS

261 Variability of the reference dataset

262 Table 2 shows the descriptive statistics of the ground-based measurements. The statistics of UAV-
 263 derived predictors are shown in Table S1 of the supplementary material.

264
 265 **Table 2** Descriptive statistics (mean \pm standard deviation (StD), minimum (Min), maximum (Max)
 266 and skewness) of the ground-measured variables on three dates together (30th October 2017; 20th
 267 November 2017; 18th November 2018): aboveground biomass (AGB), total and of weeds alone,
 268 crop height.

<i>Crop variable</i>	<i>Crop species</i>	<i>Mean \pm StD</i>	<i>Min</i>	<i>Max</i>	<i>Skewness</i>
Total AGB (g DW m ⁻²)	<i>CLO</i>	109.3 \pm 101.9	9.0	345.3	0.83
	<i>HVE</i>	152.6 \pm 100.2	20.2	376.3	0.58
	<i>OAT</i>	174.0 \pm 78.0	58.3	344.6	0.40
	<i>RYE</i>	178.2 \pm 63.1	69.8	323.9	0.27
	<i>WMU</i>	261.0 \pm 125.5	75.8	603.5	0.83
Weeds AGB (g DW m ⁻²)	<i>CLO</i>	41.5 \pm 66.3	0.0	282.1	1.75
	<i>HVE</i>	33.6 \pm 60.7	0.0	283.2	2.75
	<i>OAT</i>	10.4 \pm 16.9	0.0	56.3	1.41
	<i>RYE</i>	2.6 \pm 7.2	0.0	28.5	2.69
	<i>WMU</i>	0.1 \pm 0.9	0.0	6.1	6.50
Ground-measured	<i>CLO</i>	21.4 \pm 14.9	4.0	50.0	0.47

<i>Crop variable</i>	<i>Crop species</i>	<i>Mean ± StD</i>	<i>Min</i>	<i>Max</i>	<i>Skewness</i>
crop height (cm)	<i>HVE</i>	20.8±12.0	5.3	45.7	0.58
	<i>OAT</i>	42.9±12.0	25.0	70.0	0.67
	<i>RYE</i>	22.2±6.5	9.0	34.7	-0.21
	<i>WMU</i>	72.1±24.4	29.0	127.0	0.26

269

270 For CLO and HVE, in most cases, plants were small with the lowest AGB levels (Tab. 2), resulting
 271 in the lowest NIR reflectance values (data not shown). The highest AGB and FC were reached by
 272 OAT and WMU (Table 2; Table S1). Rye plants had high AGB levels but lower crop height. In
 273 general, the distributions of FC values showed a negative skewed distribution for all cover crop
 274 species (Table S1), indicating a higher frequency of high compared to low FC values and thus
 275 suggesting that saturating levels were reached. Descriptive statistics of the vegetation indices and
 276 crop heights (both ground-measured and UAV-based) demonstrated their high variability, adequate
 277 for calibration purposes (Table 2; Table S1).

278 UAV-derived crop height

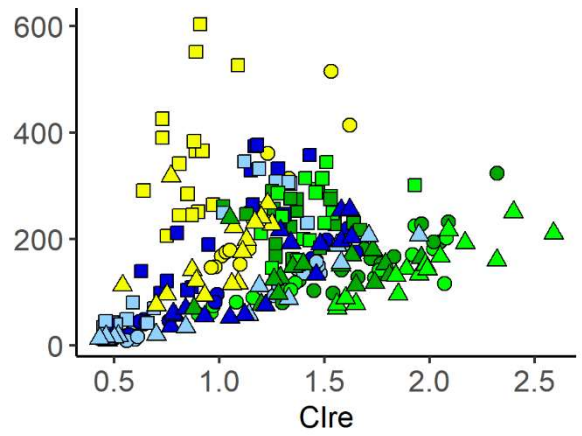
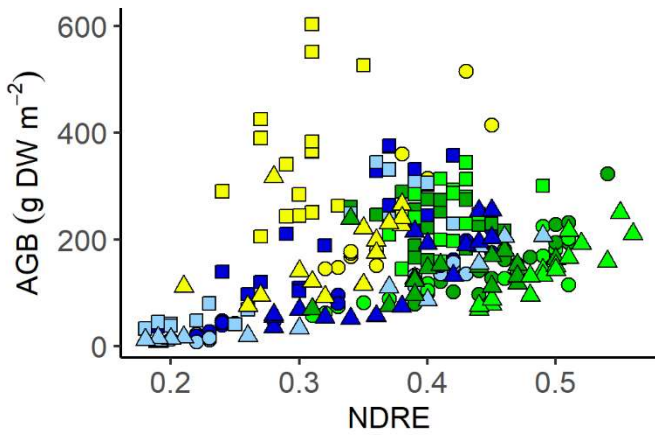
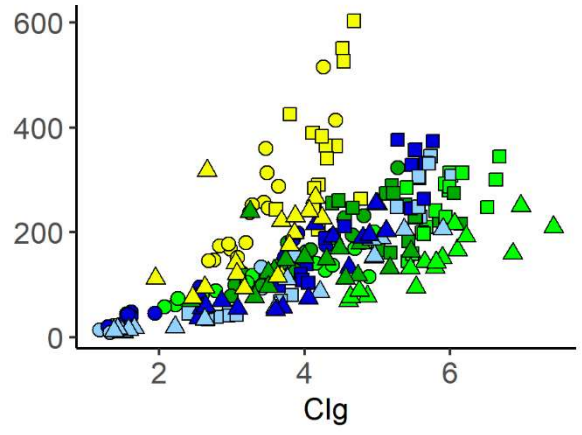
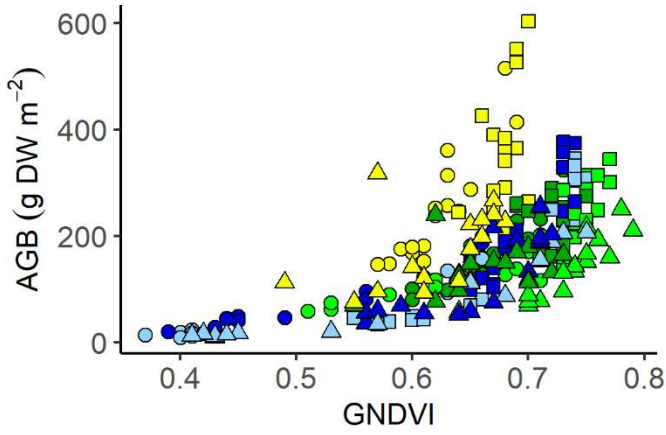
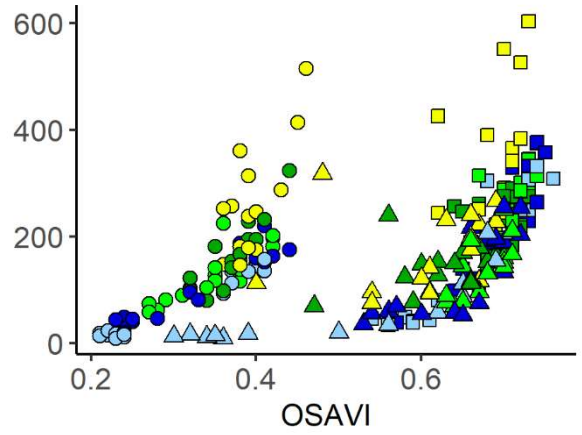
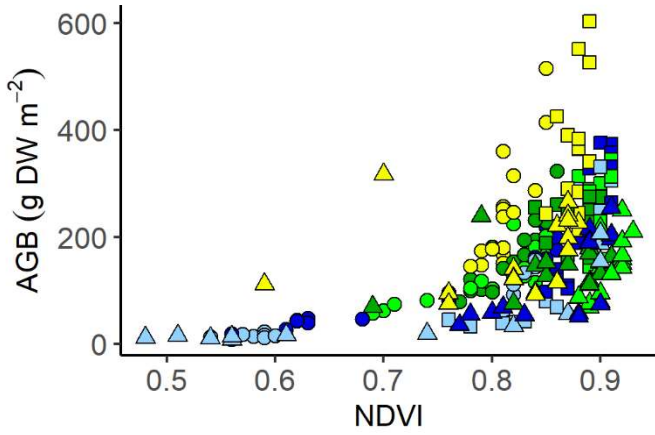
279 Ground-measured crop height was successfully estimated by UAV-derived crop height (Hest). The
 280 two measurements were linearly correlated with an R^2 of 0.8 (Fig. S1). The LOQ was also estimated
 281 by Eq. 1 and it resulted in 12.5 cm. It means that under that threshold, the UAV-crop height could
 282 not be quantified correctly. Eighteen percent of the entire dataset had a crop height under the LOQ.
 283 However, Hest bias was 8.8 cm, lower than the LOQ. This results confirmed that Hest was
 284 successfully derived by the UAV survey with the multispectral camera using the CSM method. It
 285 must be noted that the height of smaller plants could have been affected by the use of one
 286 altitude value of the bare soil for the entire field.

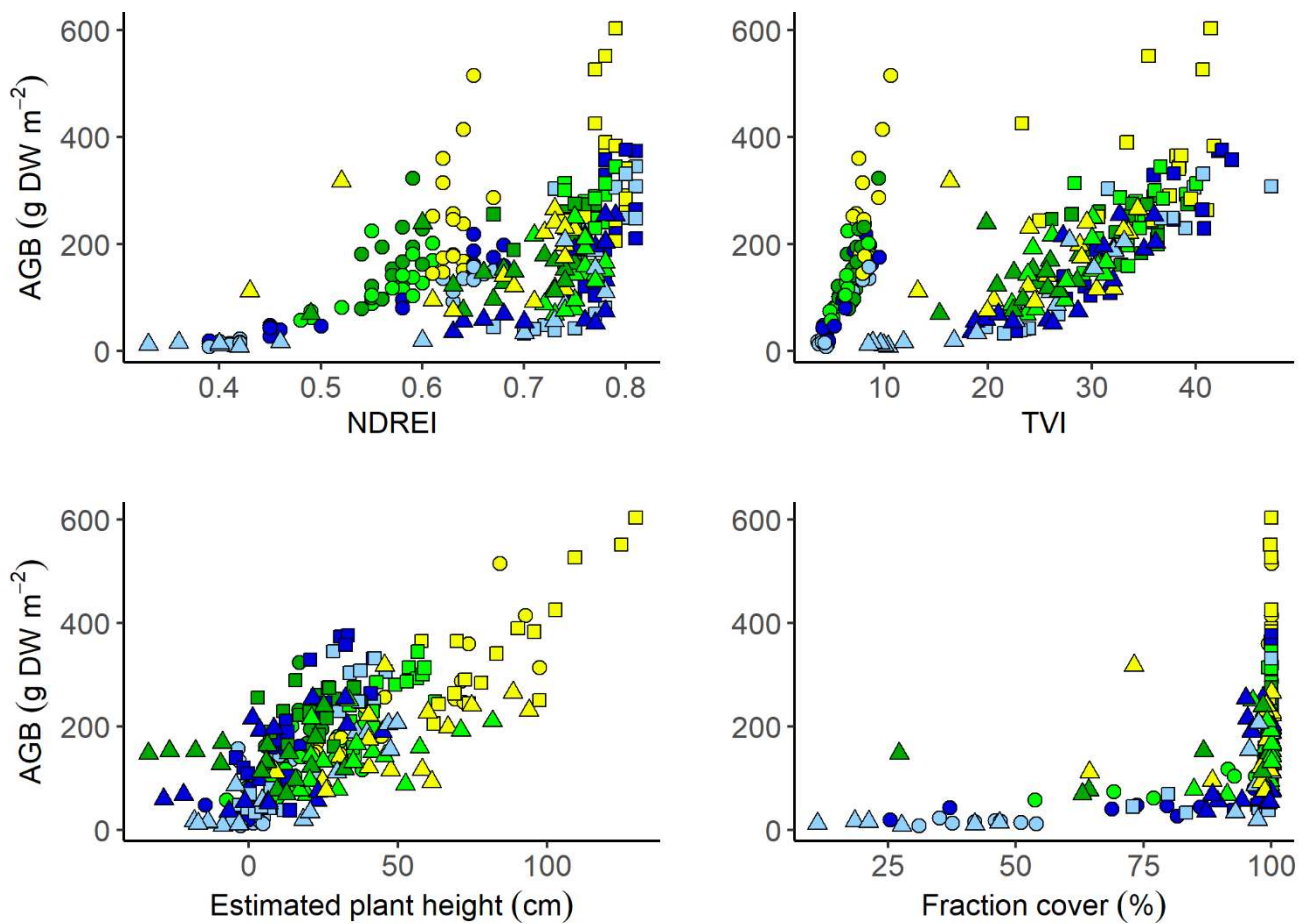
287 Simple regression models for AGB estimation

288 UAV-derived crop variables, either vegetation indices or structural properties, were tested for the
 289 estimation of AGB. Scatterplots of AGB vs. each predictor are shown in Fig. 3. Scatterplots of data
 290 divided by predictor and cover crop species are visible in Fig. S2 of the supplementary material.

Date ○ Oct2017 □ Nov2017 △ Nov2018

Cover ● CLO ● HVE ● OAT ● RYE ● WMU





291 **Fig. 3** Scatterplots of UAV-derived variables and aboveground biomass (AGB). Crop species and
 292 sampling dates have different colors and shapes, respectively. For the abbreviations of crop species,
 293 see the caption of Fig. 2.

294 *Vegetation indices as AGB predictors*

295 The best fits of simple regression models between AGB and vegetation indices were exponential
 296 and polynomial (Table 3). The statistics of all the models tested are visible in Table S2 of the
 297 supplementary material. The MAECV was much lesser than RMSECV for all crop species and
 298 calibration curves indicating overall acceptable errors. Nonetheless, nRMSECV was commented in
 299 the main text for simpler comparisons among the species-specific calibration curves.

300

301 **Table 3** Simple regression models for the estimation of aboveground biomass (AGB) of the
 302 different cover crop species from vegetation indices of all dates. The table reports the equation of

303 the best fit for each combination of index and crop species, the coefficient of determination in
 304 cross-validation (R_{cv}^2), the root mean square error in cross-validation (RMSECV), the normalized
 305 root mean square error in cross-validation (nRMSECV) and the mean absolute error (MAECV) are
 306 reported. For the abbreviations of crop species, see the caption of Fig. 2.

<i>Predictor</i>	<i>Crop</i>	<i>Best fit</i>	<i>Fitted model for AGB estimation (g DW m⁻²)</i>	R_{cv}^2	<i>RMSECV (g DW m⁻²)</i>	<i>nRMSECV (%)</i>	<i>MAECV (g DW m⁻²)</i>
NDVI	CLO	Exponential	$0.2 * e^{7.6x}$	0.85	60.2	55	41.2
	HVE	Exponential	$0.6 * e^{6.5x}$	0.66	68.9	45	50.5
	OAT	Exponential	$2.7 * e^{4.7x}$	0.38	67.0	38	52.2
	RYE	Exponential	$3.0 * e^{4.7x}$	0.35	55.2	31	44.9
	WMU	Exponential	$6.3 * e^{4.3x}$	0.35	111.8	43	84.3
OSAVI	CLO	Polynomial	$1309.7 * x^2 - 872.9 * x + 174.86$	0.60	64.2	59	53.8
	HVE	Polynomial	$1244.4 * x^2 - 893.0 * x + 226.3$	0.44	75.9	50	63.8
	OAT	Exponential	$59.6 * e^{1.7x}$	0.39	63.7	37	51.8
	RYE	Exponential	$95.6 * e^x$	0.19	58.7	33	48.7
	WMU	Polynomial	$3891.8 * x^2 - 3963.7 * x + 1183.9$	0.19	114.2	44	90.7
GNDVI	CLO*	Exponential	$0.3 * e^{8.9x}$	0.93	35.9	33	25.1
	HVE	Polynomial	$4810.5 * x^2 - 4790.7 * x + 1212.2$	0.82	45.5	30	37.7
	OAT	Exponential	$4.0 * e^{5.2x}$	0.56	56.3	32	44.3
	RYE	Exponential	$2.7 * e^{6.0x}$	0.61	45.9	26	35.2
	WMU	Exponential	$1.7 * e^{7.7x}$	0.56	90.8	35	68.7
CIg	CLO	Exponential	$5.8 * e^{0.7x}$	0.93	41.4	38	24.4
	HVE	Exponential	$14.6 * e^{0.6x}$	0.85	40.7	27	32.6
	OAT	Exponential	$38.0 * e^{0.3x}$	0.59	55.8	32	44.8
	RYE	Exponential	$44.5 * e^{0.3x}$	0.56	48.0	27	37.5
	WMU	Exponential	$32.2 * e^{0.5x}$	0.57	87.6	34	67.3
NDRE	CLO	Exponential	$2.7 * e^{10.1x}$	0.74	79.1	72	50.5
	HVE	Exponential	$8.3 * e^{7.7x}$	0.58	81.1	53	58.3
	OAT	Exponential	$50.0 * e^{2.6x}$	0.10	78.3	45	61.9
	RYE	Exponential	$84.0 * e^{1.6x}$	0.05	62.9	35	50.8
	WMU	Exponential	$112.7 * e^{2.2x}$	0.09	125.2	48	95.3
CIre	CLO	Exponential	$7.3 * e^{2.2x}$	0.71	95.7	88	57.2
	HVE	Exponential	$20.1 * e^{1.6x}$	0.55	84.5	55	60.7
	OAT	Exponential	$85.6 * e^{0.4x}$	0.09	78.5	45	62.1
	RYE	Exponential	$110.9 * e^{0.3x}$	0.06	62.6	35	50.6
	WMU	Polynomial	$373.9 * x^2 - 692.4 * x + 560.7$	0.11	121.5	47	91.4
NDREI	CLO	Exponential	$1.1 * e^{6.3x}$	0.74	68.9	63	52.4
	HVE	Exponential	$4.2 * e^{4.8x}$	0.54	75.7	50	59.9
	OAT	Exponential	$23.5 * e^{2.7x}$	0.36	66.3	38	53.6
	RYE	Exponential	$67.4 * e^{1.3x}$	0.26	56.9	32	47.0
	WMU	Exponential	$44.0 * e^{2.4x}$	0.21	116.5	45	87.0
TVI	CLO	Polynomial	$0.3 * x^2 - 5.1 * x + 70.8$	0.69	57.5	53	48.2
	HVE	Polynomial	$0.3 * x^2 - 10.2 * x + 143.0$	0.63	61.4	40	53.1
	OAT	Polynomial	$0.3 * x^2 - 8.8 * x + 162.6$	0.60	53.2	31	44.9

	RYE	Polynomial	0.3*x²-8.4*x+203.7	0.33	53.3	30	44.1
	WMU	Polynomial	0.5*x²-20.6*x+378.6	0.29	107.5	41	83.1

307 * The vegetation index with the best fit is in bold.

308

309 The green-based vegetation indices (CIg and GNDVI) had the best performance in the estimation of
310 the AGB of all the species with R_{CV}^2 of the exponential models varying from 0.56 to 0.93 and
311 nRMSECV from 26 to 38% and MAECV from 25 to 67 g DW m⁻² (Table 3). The GNDVI was the
312 best index to predict AGB of CLO and RYE (R_{CV}^2 of 0.93 and 0.61, respectively), while CIg was
313 the best predictor for HVE, OAT and WMU with R_{CV}^2 of 0.85, 0.59 and 0.57, respectively. The
314 vegetation indices showing the highest errors (nRMSECV from 35 to 88% and MAECV from 51 to
315 95 g DW m⁻²) were those based on the red-edge (CIre and NDRE). Moreover, the CIre and NDRE
316 showed a dependence on crop species and development stage, separating October 2017 and
317 November 2018 (autumn 2018 had low precipitation with less developed plants) from November
318 2017 (Fig. 3). The OSAVI, TVI and NDREI showed dependence on the timing of the survey and/or
319 FC. Specifically, they clearly separated the early sampling date from the late sampling *i.e.*, October
320 2017 *vs* November 2017 and November 2018. Finally, the NDVI had similar behavior and
321 nRMSECV to the OSAVI, TVI and NDREI, with errors from 31 to 55%. Finally, NDVI, OSAVI,
322 NDREI and GNDVI showed a saturating behavior.

323 *UAV-derived crop height and vegetation cover fraction as AGB predictors*

324 Due to the robustness of Hest and FC (structural variables) regardless of crop species, development
325 stage and timing of the survey (Fig. 3), it was possible to develop crop-specific and global (*i.e.*,
326 including all cover crops) calibration models, by fitting simple regression models on the entire
327 dataset including all species (Table 4).

328

329 **Table 4** Simple regression models for the estimation of aboveground biomass (AGB) from
330 structural predictors of all dates for different cover crop species and for the global dataset including
331 all species. The table reports the equation of the best fit for each species, the coefficient of

332 determination in cross-validation (R_{CV}^2), the root mean square error in cross-validation (RMSECV),
 333 the normalized root mean square error in cross-validation (nRMSECV) and the mean absolute error
 334 (MAECV). For the abbreviations of crop species, see the caption of Fig. 2.

<i>Predictor</i>	<i>Crop</i>	<i>Best fit</i>	<i>Fitted model for AGB estimation (g DW m⁻²)</i>	<i>R_{CV}²</i>	<i>RMSECV (g DW m⁻²)</i>	<i>nRMSECV (%)</i>	<i>MAECV (g DW m⁻²)</i>
Hest (cm)	CLO	Linear	4.3*x+53.00	0.77	65.0	59	52.0
	HVE	Polynomial	0.03*x ² +3.7*x+97.9	0.60	71.1	47	59.6
	OAT	Exponential	84.5*e ^{0.02x}	0.58	61.2	35	48.4
	RYE	Linear	1.7*x+35.7	0.25	61.5	35	53.1
	WMU	Polynomial	0.02*x ² +0.3*x+124.5	0.72	73.0	28	55.8
	Global	Linear	2.8x + 98.4	0.57	72.7	42	59.9
FC (%)	CLO	Exponential	4.4*e ^{0.03x}	0.72	79.9	73	53.2
	HVE	Exponential	5.6*e ^{0.03x}	0.51	88.7	58	68.9
	OAT	Exponential	7.4*e ^{0.03x}	0.40	69.2	40	55.4
	RYE	Exponential	64.7*e ^{0.01x}	0.26	60.3	34	49.8
	WMU	Exponential	42.8*e ^{0.02x}	0.30	124.8	48	92.3
	Global	Exponential	5.4*e^{0.03x}	0.54	94.7	54	68.2

335

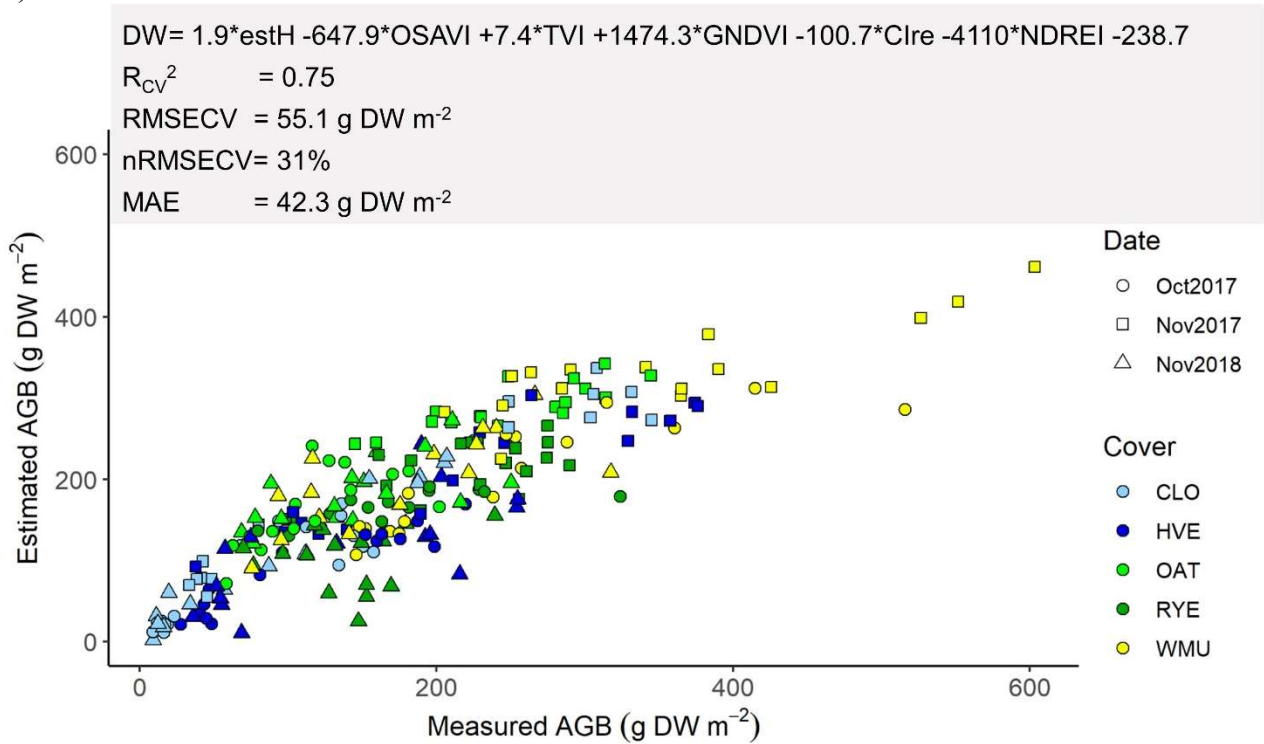
336 For WMU, crop Hest was a better estimator of AGB compared to FC and the best vegetation index
 337 (CIg), with R_{CV}^2 of 0.72, nRMSECV of 28% and the lowest MAECV (Tab. 4). The AGB of OAT
 338 was also estimated well using Hest, with performance very similar to the ones of the best vegetation
 339 index (Table 3): R_{CV}^2 of 0.58 and nRMSECV of 35% even with a slightly higher MAECV (Table
 340 4). Good results were obtained by the global calibration model: the best fit was linear with R_{CV}^2 of
 341 0.57 and nRMSECV of 42%. Finally, a global calibration was also possible for the FC (Table 4).
 342 Nonetheless, it showed a clear saturating behavior with a plateau at 97.2%, corresponding to 99.7 g
 343 DW m⁻² (Fig. 3).

344 Multiple regression models for AGB estimation

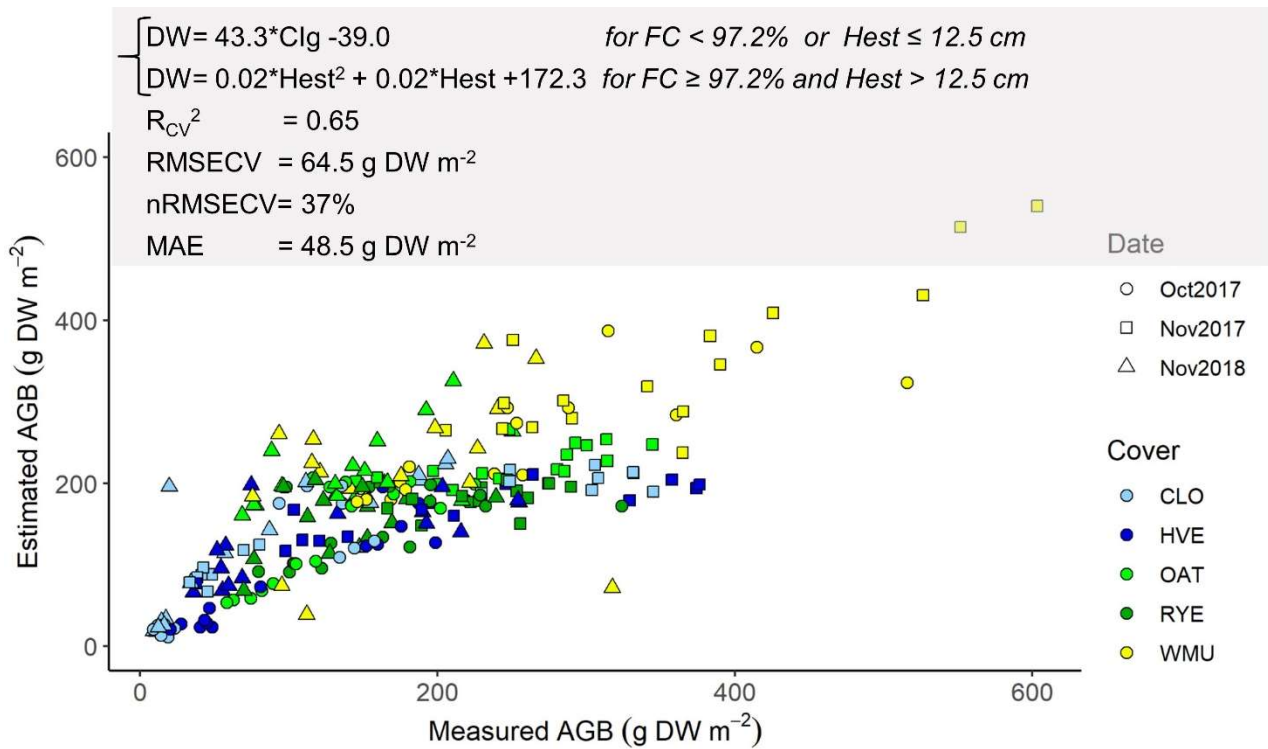
345 The calibration of the global regression models was carried out with the aim of proposing a unique
 346 equation for the estimation of AGB of various herbaceous crop species. The best multiple
 347 regression model obtained via backward stepwise regression (Fig. 4a) was better than the simple
 348 model based on Hest alone (Table 4) and showed predictive ability comparable to the models based
 349 on single vegetation indices applied to the species separately (Table 3). The model included six

350 predictors: Hest and five vegetation indices. The GNDVI was selected instead of CIg probably
351 because it better explained the variability of the AGB of RYE that was not properly estimated by
352 other vegetation indices (Table 3). Moreover, the OSAVI, TVI and NDREI, all affected by the
353 timing of the survey and/or FC, were selected as well as CIre that strongly depended on crop
354 species and development stage (Fig. 3).

a)



b)



355 **Fig. 4** Measured vs. estimated crop above-ground biomass (AGB) by multiple regression model
 356 (4a) and by a combination of regression models (4b).

357

358 The approach of using the best predictor among vegetation indices together with Hest was also
 359 tested in order to propose a simpler method able to account for the vegetation indices and structural
 360 crop properties by considering the limit of the saturation of FC and the LOQ of the Hest (12.5 cm).
 361 The CIg was chosen due to its good performances in the estimation of AGB of single species (Table
 362 3) and because of its linear correlation with AGB of the global dataset. The proposed model (Fig.
 363 4b), compared to the multiple regression model, had only a slight worsening of the R_{CV}^2 and errors,
 364 of 10% and 6%, respectively, but with the use of only three predictors (CIg and Hest; plus FC to
 365 define saturation) against the six predictors of the multiple regression model.

366 **DISCUSSION**

367 The main objective of this study was to test the combination of vegetation indices and crop
 368 structural properties to estimate the AGB of different species of crops at high levels of vegetation
 369 cover fraction.

370 Field campaigns were scheduled to guarantee the sampling of AGB at the highest levels of cover
371 crop production. In fact, even if past works on AGB estimation from vegetation indices identified
372 the saturation issue, authors did not identify and report absolute AGB values that caused the
373 saturation of vegetation indices (Huete et al., 1997; Mutanga and Skidmore 2004; Gu et al., 2013;
374 Poley and McDermid, 2020). The measured crop FC confirmed that saturation was reached at
375 97.2% of FC at 99.7 g DW m⁻² of AGB, considering all crops together.

376 However, vegetation indices showed different behavior with respect to FC suggesting that they
377 were influenced by different factors other than AGB such as leaf color, plant architecture and
378 development, and the timing of the survey. In agreement with the literature, the NDVI was the most
379 affected by saturation (Huete et al., 1997; Mutanga and Skidmore 2004; Gu et al., 2013). It
380 saturated following the same behavior of the FC, confirming the strict connection of NDVI with it.

381 Among the tested vegetation indices, the best results were reached by the green-based vegetation
382 indices (Tab. 3). The indices based on the red-edge band, CI_{re} and NDRE, showed low correlations
383 with AGB, probably due to the effect of different development stages included in the models (Fig.
384 3, Table 3), in contrast with results of other similar works (Mutanga and Skidmore 2004; Wang et
385 al., 2016). Finally, OSAVI, TVI and, in small part, NDREI, used to limit soil effects on crop
386 reflectance, showed a dependence on the timing of data acquisition (Fig. 3), contrary to previous
387 studies (Huete et al., 1997; Prabhakara et al., 2015). However, the index OSAVI was designed to
388 overcome the noise of soil brightness (Goel and Qin, 1994) and the TVI was designed to be more
389 sensitive to chlorophyll content and to be less affected by atmospheric conditions (Vincini et al.,
390 2006). These corrections could have caused the indices' values to be different in early autumn
391 (October 2017) with respect to the values of the same indices measured in November in both years,
392 considering the presence of smaller plants and the higher solar elevation angle of the sun in
393 October. For these reasons, it must be considered that an accurate atmospheric correction of UAV-
394 derived images could lead to better results (Cao et al., 2020).

395 As opposed to vegetation indices, crop height was strongly related to crop growth and it was not
396 dependent on other factors. It was evident by the linear relationship between crop height and AGB
397 with no deviations due to development stage, sampling date or species (Fig. 3). Therefore, it
398 allowed the calibration of a global model for the estimation of AGB according to attempts already
399 reported in the literature (Roth and Streit, 2018). The best fit resulted in a linear regression model
400 that proved the consistency of the correlation between crop height and AGB with no saturation even
401 at high AGB levels. Despite some issues that could arise when estimating AGB at early stages with
402 low crop heights, the good results obtained confirmed the interest in crop height as a rough
403 powerful estimator of AGB irrespective of crop species. With these premises, global calibration
404 models were also tested using all the UAV-derived variables in order to overcome the specificity of
405 AGB estimation by vegetation indices. As expected, the multiple regression model led to the best
406 results in AGB estimation (Fig. 4a). Both UAV-derived crop height and five vegetation indices
407 were selected by the model, indicating that the combination of vegetation indices and structural
408 crop properties improved the estimation of AGB. Similar results were obtained in previous studies
409 that tested the ability of multiple linear and non-linear regression models using crop height and
410 vegetation indices to estimate AGB of cereal crops (Bendig et al., 2014; Bendig et al., 2015;
411 Marshall and Thenkabail, 2015; Tilly et al., 2015). The vegetation indices selected by the backward
412 procedure of the multiple regression model were those affected by crop species and/or development
413 stage (CI_{re}) or FC and/or timing of the survey (TVI, OSAVI and NDREI), other than GNDVI, that,
414 with CI_g, was the best index to predict AGB. This result pointed out the need for predictors that
415 accounted for the difference among species and development stages in order to explain the
416 variability of the collected dataset. However, according to the literature, we observed that, when
417 plants are very small with dense canopies, vegetation indices (specifically, the green-based indices)
418 are very sensitive to differences in crop growth and are suitable for the estimation of AGB (Tilly et
419 al., 2015; Roth and Streit, 2018). Otherwise, when plants have a vertical growth and FC is saturated,
420 crop height is the best estimator of AGB. For the abovementioned reasons, a new regression

421 approach was proposed for the first time in this study (Fig. 4b). It combined two predictors: the best
422 vegetation index (in terms of AGB prediction) was used to predict AGB until FC saturation
423 occurred or when the Hest was under the estimated LOQ. Otherwise, Hest was used. The proposed
424 method overcomes the saturation phenomenon by using vegetation indices at low FC levels when
425 they have the power to detect small changes in soil coverage and use Hest when it is maximally
426 related to AGB when FC is high and vegetation indices lose their ability to detect changes in AGB,
427 also caused by crop vertical growth. Moreover, the use of different regression models for different
428 predictors overcame the overfitting that could have affected the multiple regression model that was
429 applied on correlated predictors, in this case the vegetation indices ($r= 0.10-0.97$, Table S3).
430 In this context, the results were very promising. Statistics in cross-validation showed a small
431 decrease with respect to the multiple regression model (Fig. 4) if compared to the decrease in the
432 number of predictors (two uncorrelated *vs.* six correlated, respectively). Moreover, the results were
433 comparable to the performance of regression models of studies that proposed multiple regression
434 approaches on only one crop species (Bendig et al., 2014; Bendig et al., 2015; Marshall and
435 Thenkabail, 2015; Tilly et al., 2015) confirming the possibility of overcoming the specificity of
436 vegetation indices in the estimation of AGB and producing advancement with respect to previous
437 works on similar herbaceous crops that did not explore the combination of the vegetation indices
438 and structural crop properties for the estimation of AGB (Roth and Streit, 2018).

439 Future perspectives

440 As a result of this work, two crucial aspects for the improvement of the estimation of herbaceous
441 crop AGB emerged. Firstly, a larger dataset with more variability in the initial crop growth stages
442 and different plant habits is fundamental to extend the proposed calibration models and to prove the
443 robustness of the proposed approaches. Secondly, different ways to estimate crop height also at
444 early crop development stages should be studied with different sensors on crops with different plant
445 habits to retrieve reliable crop height estimates in operational conditions. In fact, this study
446 confirmed that plant height can be successfully estimated by UAV-derived CSMs (Roth and Streit,

447 2018; Poley and McDermid, 2020). However, crop height estimation from airborne images should
448 be improved. Specifically, our results showed that the LOQ of the estimation of crop height was
449 12.5 cm. Moreover, it must be considered that an average altitude of the field was used to estimate
450 crop heights, so the height and AGB of small plants with horizontal habits were difficult to
451 quantify. To gain even better results, more accurate methods of estimating plant height should be
452 considered *e.g.*, having reference altitudes measured in the fields (more than 30 points) to build
453 digital terrain models or making an aerial survey of the bare soil of the field. Finally, different
454 technologies should be considered such as LiDAR (Deery et al., 2014; Wiering et al., 2019) or
455 ultrasonic sensors mounted on tractors (Farooque et al., 2013) as well as more resolved imaging
456 sensors such as RGB cameras with very high spatial resolutions.

457 **CONCLUSIONS**

458 The estimation of herbaceous crop aboveground biomass was tested using both vegetation indices
459 and structural crop properties. It was estimated by green-based vegetation indices with varying
460 degrees of success for the different crop species ($R_{CV}^2= 0.56-0.93$, $nRMSECV= 26-38\%$). Also,
461 plant height was a good estimator of aboveground biomass with a more linear correlation to it.
462 Consequently, at first, we used crop height for the calibration of a global model for AGB estimation
463 of all species together, regardless of the development stage, the timing of the survey and vegetation
464 cover fraction, with good results ($R_{CV}^2= 0.57$, $nRMSECV= 42\%$). Even if with slightly worse
465 performance, a global curve for aboveground biomass estimation is more interesting for simplicity
466 and possibility of integrating new data of species, timings and localities, than a species-specific
467 equation for application in real fields. For these reasons, and for the different nature and
468 performance of the vegetation indices and structural crop properties, we attempted to calibrate
469 global multiple regression models that combine various properties for AGB estimation. Firstly, the
470 calibration of a backward stepwise linear regression model led to the estimation of AGB with $R_{CV}^2=$
471 0.75 and $nRMSECV= 31\%$ using six predictors. These were Hest and five vegetation indices.

472 Secondly, a combined regression model was built using two predictors only, CIG (before saturation,
473 defined using the fraction cover) and Hest (after saturation). This simple model showed
474 encouraging results with $R_{CV}^2 = 0.65$ and $nRMSECV = 37\%$, suggesting that combining vegetation
475 indices and structural crop variables (such as crop height) could improve the estimation of AGB by
476 overcoming the specificity of vegetation indices. Moreover, its simplicity makes it preferable to
477 other complex models for application in real conditions. Nonetheless, the integration of vegetation
478 indices, crop height and fraction cover should be studied over a wider range of aboveground
479 biomass levels, crop species and vegetation indices to produce a robust approach for the estimation
480 of aboveground biomass.

481 **CONFLICT OF INTEREST**

482 The authors declare that they have no conflict of interest.

483 **DATA AVAILABILITY**

484 The datasets generated during and analysed during the current study are available from the
485 corresponding author on reasonable request.

486 **REFERENCES**

- 487 Azimi, S., Kaur, T., Gandhi, T.K., 2021. A deep learning approach to measure stress level in plants
488 due to nitrogen deficiency. *Measurement* 173, 108650.
489 <https://doi.org/10.1016/j.measurement.2020.108650>
- 490 Bendig, J., Bolten, A., Bennertz, S., Broscheit, J., Eichfuss, S., Bareth, G., 2014. Estimating
491 biomass of barley using crop surface models (CSMs) derived from UAV-based RGB imaging.
492 *Remote Sensing* 6, 10395–10412. <https://doi.org/10.3390/rs61110395>
- 493 Bendig, J., Yu, K., Aasen, H., Bolten, A., Bennertz, S., Broscheit, J., et al., 2015. Combining UAV-
494 based plant height from crop surface models, visible, and near infrared vegetation indices for

495 biomass monitoring in barley. *International Journal of Applied Earth Observation and*
496 *Geoinformation* 39, 79–87. <https://doi.org/10.1016/j.jag.2015.02.012>

497 Calou, V.B., Teixeira, A. dos S., Moreira, L.C., Rocha Neto, O.C. da, Silva, J.A. da, 2019.
498 Estimation of maize biomass using unmanned aerial vehicles. *Engenharia Agrícola* 39, 744–752.
499 <http://dx.doi.org/10.1590/1809-4430-eng.agric.v39n6p744-752/2019>

500 Cao, H., Gu, X., Wei, X., Yu, T., Zhang, H., 2020. Lookup Table Approach for Radiometric
501 Calibration of Miniaturized Multispectral Camera Mounted on an Unmanned Aerial Vehicle.
502 *Remote Sensing* 12, 4012. <https://doi.org/10.3390/rs12244012>

503 Corti, M., Gallina, P.M., Cavalli, D., Cabassi, G., 2017. Hyperspectral imaging of spinach canopy
504 under combined water and nitrogen stress to estimate biomass, water, and nitrogen content.
505 *Biosystems Engineering* 158, 38–50. <https://doi.org/10.1016/j.biosystemseng.2017.03.006>

506 Corti, M., Cavalli, D., Cabassi, G., Gallina, P.M., Bechini, L., 2018. Does remote and proximal
507 optical sensing successfully estimate maize variables? A review. *European Journal of Agronomy*
508 99, 37–50. <https://doi.org/10.1016/j.eja.2018.06.008>

509 Corti, M., Marino Gallina, P., Cavalli, D., Ortuani, B., Cabassi, G., Cola, G., et al., 2020.
510 Evaluation of in-season management zones from high-resolution soil and plant sensors.
511 *Agronomy* 10, 1124. <https://doi.org/10.3390/agronomy10081124>

512 Deery, D., JimenezBerni, J., Jones, H., Sirault, X., Furbank, R., 2014. Proximal remote sensing
513 buggies and potential applications for field-based phenotyping. *Agronomy* 4, 349–379.
514 <https://doi.org/10.3390/agronomy4030349>

515 Farooque, A.A., Chang, Y.K., Zaman, Q.U., Groulx, D., Schumann, A.W., Esau, T.J., 2013.
516 Performance evaluation of multiple ground based sensors mounted on a commercial wild
517 blueberry harvester to sense plant height, fruit yield and topographic features in real-time.
518 *Computers and Electronics in Agriculture* 91, 135–144.
519 <https://doi.org/10.1016/j.compag.2012.12.006>

520 Freeman, K.W., Girma, K., Arnall, D.B., Mullen, R.W., Martin, K.L., Teal, R.K., et al., 2007. By-
521 plant prediction of corn forage biomass and nitrogen uptake at various growth stages using
522 remote sensing and plant height. *Agronomy Journal* 99, 530–536.
523 <https://doi.org/10.2134/agronj2006.0135>

524 Goel, N.S., Qin, W., 1994. Influences of canopy architecture on relationships between various
525 vegetation indices and LAI and FPAR: A computer simulation. *Remote Sensing Reviews* 10,
526 309–347. <https://doi.org/10.1080/02757259409532252>

527 Gu, Y., Wylie, B.K., Howard, D.M., Phuyal, K.P., Ji, L., 2013. NDVI saturation adjustment: A new
528 approach for improving cropland performance estimates in the Greater Platte River Basin, USA.
529 *Ecological Indicators* 30, 1–6. <https://doi.org/10.1016/j.ecolind.2013.01.041>

530 Haboudane, D., Miller, J.R., Tremblay, N., ZarcoTejada, P.J., Dextraze, L., 2002. Integrated
531 narrowband vegetation indices for prediction of crop chlorophyll content for application to
532 precision agriculture. *Remote Sensing of Environment* 81, 416–426.
533 [https://doi.org/10.1016/S00344257\(02\)000184](https://doi.org/10.1016/S00344257(02)000184)

534 Huete, A.R., Liu, H., van Leeuwen, W.J., 1997. The use of vegetation indices in forested regions:
535 issues of linearity and saturation. In IEEE *International Geoscience and Remote Sensing*
536 *Symposium Proceedings*, vol 4, pp. 1966–1968. <https://doi.org/10.1109/IGARSS.1997.609169>

537 Jackson, R.D, Huete, A.R., 1991. Interpreting vegetation indices. *Preventive Veterinary Medicine*
538 11, 185. [https://doi.org/10.1016/S0167-5877\(05\)80004-2](https://doi.org/10.1016/S0167-5877(05)80004-2)

539 Jimenez-Berni, J.A., Deery, D.M., RozasLarraondo, P., Condon, A. (Tony) G., Rebetzke, G.J.,
540 James, R.A., et al., 2018. High-throughput determination of plant height, ground cover, and
541 aboveground biomass in wheat with LiDAR. *Frontiers in Plant Science* 9, 237.
542 <https://doi.org/10.3389/fpls.2018.00237>

543 Kuhn, M., 2021. caret: Classification and Regression Training. R package version 6.0-90. Retrieved
544 date (month/year) from <https://CRAN.R-project.org/package=caret>

545 Lumley, T., based on Fortran code by Alan Miller, 2020. leaps: Regression Subset Selection. R
546 package version 3.1. Retrieved date (month/year) from [https://CRAN.R-](https://CRAN.R-project.org/package=leaps)
547 [project.org/package=leaps](https://CRAN.R-project.org/package=leaps)

548 Madec, S., Baret, F., De Solan, B., Thomas, S., Dutartre, D., Jezequel, S., et al., 2017. High-
549 throughput phenotyping of plant height: comparing unmanned aerial vehicles and ground LiDAR
550 estimates. *Frontiers in Plant Science* 8, 2002. <https://doi.org/10.3389/fpls.2017.02002>

551 Marshall, M., Thenkabail, P., 2015. Developing in situ Non-Destructive Estimates of Crop Biomass
552 to Address Issues of Scale in Remote Sensing. *Remote Sensing* 7, 808–835.
553 <https://doi.org/10.3390/rs70100808>

554 Muggeo, V.M., 2008. Segmented: an R package to fit regression models with broken-line
555 relationships. *R news* 8, 20–25. Retrieved date (month/year) from
556 [https://www.researchgate.net/publication/234092680_Segmented_An_R_Package_to_Fit_Regre-](https://www.researchgate.net/publication/234092680_Segmented_An_R_Package_to_Fit_Regression_Models_With_Broken-Line_Relationships)
557 [ssion_Models_With_Broken-Line_Relationships](https://www.researchgate.net/publication/234092680_Segmented_An_R_Package_to_Fit_Regression_Models_With_Broken-Line_Relationships)

558 MuñozHuerta, R., GuevaraGonzalez, R., ContrerasMedina, L., TorresPacheco, I., PradoOlivarez, J.,
559 OcampoVelazquez, R., 2013. A review of methods for sensing the nitrogen status in plants:
560 advantages, disadvantages and recent advances. *Sensors* 13, 10823–10843.
561 <https://doi.org/10.3390/s130810823>

562 Mutanga, O., Skidmore, A.K., 2004. Narrow band vegetation indices overcome the saturation
563 problem in biomass estimation. *International Journal of Remote Sensing* 25, 3999–4014.
564 <https://doi.org/10.1080/01431160310001654923>

565 Noh, H., Zhang, Q., Han, S., Shin, B., Reum, D., 2005. Dynamic calibration and image
566 segmentation methods for multispectral imaging crop nitrogen deficiency sensors. *Transactions*
567 *American Society of Agricultural Engineers* 48, 393–401. <https://doi.org/10.13031/2013.17933>

568 Otsu, N., 1975. A threshold selection method from gray-level histograms. *Automatica* 11, 23–27.
569 <https://doi.org/10.1109/TSMC.1979.4310076>

570 Pauly, K., 2016. Towards calibrated vegetation indices from UAS-derived orthomosaics. In
571 *Proceedings of the 13th International Conference on Precision Agriculture*. Retrieved date
572 (month/year) from

573 Pinter Jr, P.J., Hatfield, J.L., Schepers, J.S., Barnes, E.M., Moran, M.S., et al., 2003. Remote
574 sensing for crop management. *Photogrammetric Engineering & Remote Sensing* 69, 647–664.
575 <https://doi.org/10.14358/PERS.69.6.647>

576 Poley, L.G., McDermid, G.J., 2020. A systematic review of the factors influencing the estimation of
577 vegetation aboveground biomass using unmanned aerial systems. *Remote Sensing* 12, 1052.
578 <https://doi.org/10.3390/rs12071052>

579 Prabhakara, K., Hively, W.D., McCarty, G.W., 2015. Evaluating the relationship between biomass,
580 percent groundcover and remote sensing indices across six winter cover crop fields in Maryland,
581 United States. *International Journal of Applied Earth Observation and Geoinformation* 39, 88–
582 102. <https://doi.org/10.1016/j.jag.2015.03.002>

583 QGIS.org, 2020. QGIS Geographic Information System. QGIS Association. <http://www.qgis.org>

584 R Core Team, 2019. R: A language and environment for statistical computing. R Foundation for
585 Statistical Computing, Vienna, Austria. <https://www.Rproject.org/>

586 Rasmussen, J., Ntakos, G., Nielsen, J., Svendsgaard, J., Poulsen, R.N., Christensen, S., 2016. Are
587 vegetation indices derived from consumer-grade cameras mounted on UAVs sufficiently reliable
588 for assessing experimental plots? *European Journal of Agronomy* 74, 75–92.
589 <https://doi.org/10.1016/j.eja.2015.11.026>

590 Revelle W (2020). psych: Procedures for Psychological, Psychometric, and Personality Research.
591 Northwestern University, Evanston, Illinois, USA. R package version 2.0.9, Retrieved date
592 (month/year) from <https://CRAN.Rproject.org/package=psych>

593 Roth, L., Streit, B., 2018. Predicting cover crop biomass by lightweight UAS-based RGB and NIR
594 photography: an applied photogrammetric approach. *Precision Agriculture* 19, 93–114.
595 <https://doi.org/10.1007/s11119-017-9501-1>

596 Sharma, L.K., Bu, H., Franzen, D.W., Denton, A., 2016. Use of corn height measured with an
597 acoustic sensor improves yield estimation with ground based active optical sensors. *Computers*
598 *and Electronics in Agriculture* 124, 254–262. <https://doi.org/10.1016/j.compag.2016.04.016>

599 Shrivastava, A., Gupta, V.B., 2011. Methods for the determination of limit of detection and limit of
600 quantitation of the analytical methods. *Chronicles of Young Scientists* 2, 21.
601 <https://doi.org/10.4103/2229-5186.79345>

602 Thenkabail, P.S., Smith, R.B., De Pauw, E., 2000. Hyperspectral vegetation indices and their
603 relationships with agricultural crop characteristics. *Remote sensing of Environment* 71, 158–182.
604 [https://doi.org/10.1016/S0034-4257\(99\)00067-X](https://doi.org/10.1016/S0034-4257(99)00067-X)

605 Tilly, N., Aasen, H., Bareth, G., 2015. Fusion of plant height and vegetation indices for the
606 estimation of barley biomass. *Remote Sensing* 7, 11449–11480.

607 Vincini, M., Frazzi, E., D’Alessio, P., 2006. Angular dependence of maize and sugar beet VIs from
608 directional CHRIS/Proba data. In *Proceedings of 4th ESA CHRIS PROBA Workshop*, pp. 19–21.
609 Retrieved date (month/year) from
610 https://www.researchgate.net/profile/Ermes_Frazzi/publication/228413259_Angular_dependence_of_maize_and_sugar_beet_VIs_from_directional_CHRISProba_data/links/0046352d50c18b3fe6000000/Angular-dependence-of-maize-and-sugar-beet-VIs-from-directional-CHRIS-Proba-data.pdf

613

614 Wang, C., Feng, M.C., Yang, W.D., Ding, G.W., Sun, H., Liang, Z.Y., et al., 2016. Impact of
615 spectral saturation on leaf area index and aboveground biomass estimation of winter wheat.
616 *Spectroscopy Letters* 49, 241–248. <https://doi.org/10.1080/00387010.2015.1133652>

617 Wickham, H., 2016. *ggplot2: Elegant Graphics for Data Analysis*. Springer-Verlag New York.
618 ISBN 9783319242774, Retrieved date (month/year) from <https://ggplot2.tidyverse.org>

619 Wiering, N.P., Ehlke, N.J., Sheaffer, C.C., 2019. Lidar and RGB Image Analysis to Predict Hairy
620 Vetch Biomass in Breeding Nurseries. *The Plant Phenome Journal* 2, 190003.
621 <https://doi.org/10.2135/tppj2019.02.0003>

